Using Log-Gabor Filter Array to Estimate Seismic Dip and Azimuth

Yingwei Yu*, Cliff Kelley, and Irina Mardanova, IHS Global, Inc.

This paper was prepared for presentation during the 14th International Congress of the Brazilian Geophysical Society held in Rio de Janeiro, Brazil, August 3-6, 2015.

Abstract

In this paper, we introduce a method of orientation estimation in seismic data. Unlike conventional methods of orientation estimation with a context window, our method is inspired by the neural mechanism of visual perception. The primary visual cortex in the brain contains orientation columns, which are composed of an array of orientation detectors. A log-Gabor filter with a specific orientation and scale configuration simulates the neuronal mechanism of the orientation detector, while an array of such filters simulates the orientation columns. The resulting orientation is derived at the sample level of the input seismic data: the filter response competes with each other in the array, and the maximum response defines the seismic orientation. Our proposed method has many applications in seismic interpretation, e.g., calculating the volumetric azimuth and dip attributes without picking, guiding seismic attribute computation, and detecting seismic texture patterns.

Orientation Analysis in Seismic Interpretation

The orientation patterns in a seismic image, such as the dip and azimuth attributes, serve as very important tools for 3D seismic data interpretation (Chopra and Marfurt, 2007). They can highlight subtle faults and fractures (Barnes, 2003) or provide guidance for horizon auto-picking (Yu et al., 2011). Moreover, many seismic attributes are calculated either based on or guided by the orientation structures in the seismic image. For example, the attributes of the volumetric curvature and reflector shape are derived from the dip and azimuth volumes. Some other seismic attributes, such as coherence, can be guided by the orientation structure. Bakker (2002) used gradient structure tensor (GST) to get the dip, and calculated the coherence with a dip-steered context window, which is the dip-scan coherence. Aqrawi and Boe (2011) used a dip guided and modified 3D Sobel filter to highlight the fault and fracture features in seismic data.

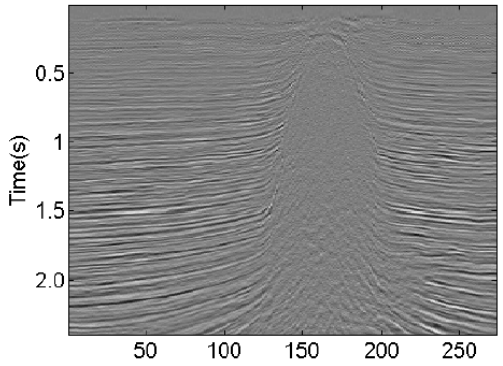

(a) Amplitude Slice from a Salt Dome Survey

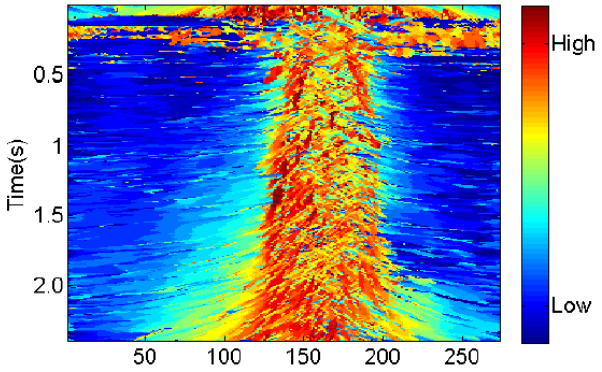

(b) Dip Calculated from the Seismic Image in (a)

Figure 1: **Amplitude and Dip of a Salt Dome Seismic Image.** Seismic survey data courtesy of FairfieldNodal. The method to generate the dip attribute in (b) is demonstrated as the first experiment in the third section.

There have been some significant advances in calculating volumetric dip and azimuth for 3D seismic data without picking any horizon. For examples, Luo et al. (1996) and Barnes (1996) estimated vector dip based on a 3D extension of the analytic trace. Marfurt et al. (1998) proposed a dip calculating method by discrete scans. Bakker et al. (1999) proposed the GST method to calculate the apparent dips. See (Chopra and Marfurt, 2007, see chap. 2) for a comprehensive summary of these methods. However, all the above methods are context window-based methods in spatial domain, and sensitive to the background noise. Our proposed method is different in that the orientation pattern is analyzed in frequency domain, and inspired by the neuronal circuits in the biological brain. Our method simulates the robust mechanism by which humans perceive orientation patterns from a natural image. 2D vectors calculated along the inline and crossline directions.

The Motivation: Neuronal Responses for Orientation Perception

Our proposed method is inspired by the biological brain's keen ability to identify orientation patterns in vision. Thus it motivated us to study the neuronal circuits for orientation detection, and apply them to seismic image analysis.

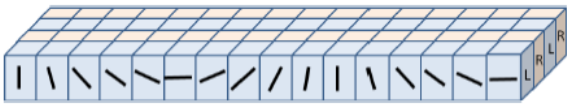

Figure 2: **The Orientation Columns in the Primary Visual Cortex.** Redrawn from Hubel and Wiesel (1959).

Hubel and Wiesel (1959) proposed the ice-cube model of the primary visual cortex like the one in Figure 2 by observing the cat's striate cortex. As in the model, the visual cortex area is composed by a slab of orientation detectors (simple cells), which are tuned in the responses to different orientation patterns. The perceived angle in the visual input pattern is then determined by the strength of the orientation detectors' responses. In the following analysis, we will model the orientation detectors with an orientation-tuned filter, and use an array of such filters to simulate the orientation column to estimate the perceived orientation.

The rest of this paper is organized as follows. The next section introduces our methods to derive the orientation vector field from the input seismic data. Experiments and results are exposed in the third section, followed by a conclusion.

Methods

In this section, we first introduce the simulation of an orientation detector using a log-Gabor filter. Then we will build the orientation column as an array of such filters. According to the activation profile of an orientation column, we can derive the perceived orientation from the filter with the maximum response. The result of the orientation detection method is to generate an orientation vector field (OVF), which indicates both directions and magnitudes of the orientation patterns from the input image.

Simulating the Orientation Detector: Log-Gabor Filter

Daugman (1980) first modeled the orientation detectors as a 2D form Gabor wavelet, which is often used as an orientation detector in many applications in the realm of imaging processing (see Jain et al., 1997). Field (1987) proposed an alternative to the Gabor filter, the log-Gabor filter, which is an improved version. The log-Gabor filter has no direct current (DC) component, and overcomes the bandwidth limitation in the conventional Gabor filter.

As proposed by Field (1987), natural images have a frequency distribution as Gaussian in logarithmic scale and the log-Gabor filter has the required logarithmic Gaussian profile. The seismic data follows the rule of natural images. Figure 3 shows the frequency plot of one trace from the salt dome seismic data in Figure 1. The frequency distribution reflects the logarithmic Gaussian patterns. The 2D log-Gabor filter is defined in frequency domain as follows (Field, 1987):

$$H(f,\alpha) = H_f \times H_\alpha, \quad (1)$$

where H_f is a radial component (see Figure 4a), and $H\alpha$ is an angular component (see Figure 4b). The radial component is 2D Gaussian in logarithmic scale, and the angular component is Gaussian along orientations. More specifically,

$$H(f,\alpha) = exp\left(-\frac{ln^2(f/f_0)}{2ln^2(\sigma_f/f_0)}\right) \times exp\left(-\frac{(\alpha-\theta)^2}{2\sigma_\alpha^2}\right), \quad (2)$$

where f_0 is central frequency, and θ is the filter direction.

Modeling the Orientation Column: log-Gabor Filter Array

A single orientation detector can respond maximally to a specific angle, but cannot tell the exact angle in the input. It is the orientation column, i.e., an array of orientation detectors that perceive the orientation patterns. First we study how orientation columns in the visual cortex interact in response to orientation patterns and then build the model of it to derive the OVF. For an orientation pattern with a specific angle, there

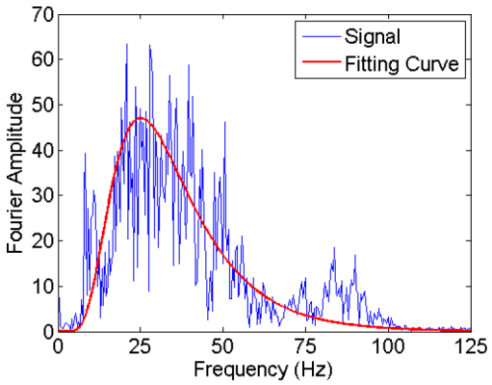

Figure 3: **The Power Spectrum of the Seismic Data Overlay with A Logarithmic Gaussian Curve**. One trace from the salt dome seismic data is transformed into frequency domain by DFFT. The x-axis is frequency and y-axis represents the strength of frequency responses. It shows that the seismic data's spectrum (blue) follows the logarithmic Gaussian distribution (red) with σ_f = 15.41 and f_0 = 25.

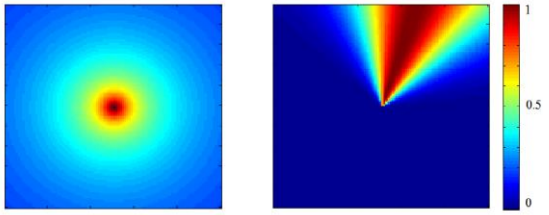

(a) Radial Component (b) Angular Component

Figure 4: **Log-Gabor Filter in Frequency Domain.** (a) Radial component: 2D Gaussian in logarithmic scale. (b) Angular component: Gaussian along orientations.

is a corresponding orientation detector in an orientation column that responds maximally, and the orientation column responses can be approximated by Gaussian distributions (Martinez et al., 2002). In Figure 5, the activation of orientation detectors in an orientation column in response to two angles is shown. The dashed curve is the response of the cells in an orientation column (x-axis) to a zero-degree line, while the solid curve is that to a 30 degree line (Yu and Choe, 2008). It shows that all of the orientation detectors tuned to various angles give responses to an input, and the perceived angle is determined by the detector with the peak response in the orientation column.

Daugman (1980) first employed a bank of Gabor filters centered at different orientations and scales in the frequency domain for image analysis. Others used a set of Gabor filters with similar configurations for texture analysis (Bovik et al., 1990), or image compression (Lee, 1996). Recently, Fischer et al. (2007) proposed an array of multi-resolution log-Gabor filters that centered on a number of orientations for image representation, and successfully applied it to image denoise and compression. We adapted the approach of Fischer et al. (2007) to simulate the orientation column. Instead of image representation, our method is designed for orientation analysis. The resulting OVF can be derived as follows.

For an input 2D seismic image in the spatial domain *I (x,y),* first apply a Fourier transform into the frequency domain $\hat{I}$ (*u,v*). The application of log-Gabor filter in the frequency domain is,

$$\hat{Y}^{<w,\theta>}(u,v) = H^{<w,\theta>}(u,v)\hat{I}(u,v), \qquad (3)$$

where H is the log-Gabor filter with orientation q and central frequency w. Since it is an array of log-Gabor filters, their central orientations q can be in a series of orientations, such as $\{-\frac{\pi}{2}, -\frac{5\pi}{8}, -\frac{\pi}{4}, \ldots, +\frac{\pi}{4}, \frac{5\pi}{8}\}$, and *w* can be in single or multiple scales as well.

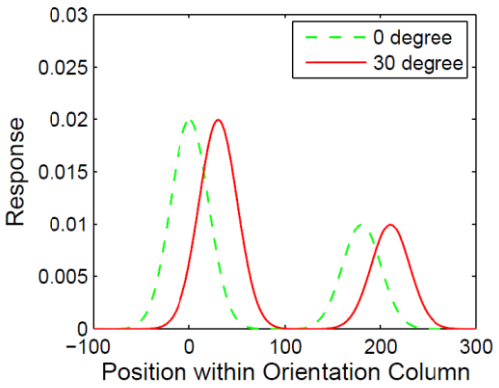

Figure 5: **Orientation Column Activation Profile**. The activation of orientation detectors in response to two angles is shown. The dashed curve is the response of the cells in an orientation column (x-axis) to a zero-degree line, and the solid curve that of a 30 degree line. Adapted from Yu and Choe (2008).

By inverse Fourier transform, we convert $\hat{Y}^{<w,\theta>}u(u,v)$ into a complex image in the spatial domain. The resulting convolved image has a real part, $Y_r^{<w,\theta>}(u,v)$, and an imaginary part, $Y_{im}^{<w,\theta>}(u,v)$. The norm of the complex image is called orientation energy in the specific orientation q and scale w:

$$Y^{<w,\theta>}(x,y) = \sqrt{[Y_r^{<w,\theta>}(x,y)]^2 + [Y_{im}^{<w,\theta>}(x,y)]^2}. \qquad (4)$$

As indicated by the observed activation profile, when we line up all the filter responses for an individual pixel at *(x,y),* we can derive the perceived orientation at this point by getting the location of peak responses in the orientation column. In the model, the most salient orientation pattern γ at pixel *(x,y)* is defined by the index of the peak value of the summed orientation responses in all scales:

$$\gamma(x,y) = \arg\max_{\theta} \sum_{w} Y^{<w,\theta>}(x,y). \qquad (5)$$

The γ*(x,y)* is also referred to as the apparent dip (Chopra and Marfurt, 2007). It is one of the two components of the OVF in the output, the other is the orientation energy *E(x,y),* which is the sum of filter responses with the orientation *γ(x,y)* in all scales:

$$E(x,y) = \sum_{w} Y^{<w,\gamma(x,y)>}(x,y). \qquad (6)$$

The orientation energy E reflects the strength of orientation features. The low values of orientation energy mean that there are fewer oriented patterns in the neighborhood, while the stronger
ones mean the orientation feature is more salient in the context. Figure 6 shows an example of the OVF generated for a 2D seismic slice near a salt dome.

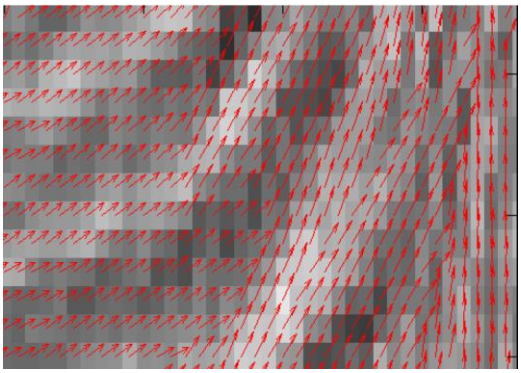

Figure 6: **Orientation Vector Field Near a Salt Dome**. The orientation vectors (red) are plotted on top of the seismic image in a region near the salt dome. The magnitudes of the vectors are normalized.

Results

The described algorithm was tested on a 3D seismic survey containing a salt dome in the center as shown in Figure 1. In the first experiment, we first generate the OVF from the amplitude volume, and use the orientation component to derive the dip and azimuth attributes. In the second experiment, we examine the orientation energy component in the resulting OVF from the salt dome seismic survey. In both experiments, the filter array contains eight log-Gabor filters, whose orientations are from $-\frac{\pi}{2}$ to $\frac{\pi}{2}$ with angle interval of $\frac{\pi}{8}$, and central frequencies are at 25 Hz.

In the experiment, the volumetric dip and azimuth attributes are derived from the orientation vectors in OVF. We first generate the OVF of the seismic amplitude volume in both inline and cross-line slices as shown in Figure 6. The instantaneous azimuth ϕ can be derived from the apparent dips in inline γ_x and cross-line γ_y as follows (Chopra and Marfurt, 2007):

$$\phi = \arctan\left(\frac{\tan\gamma_x}{\tan\gamma_y}\right), \qquad (7)$$

and the instantaneous dip θ is then derived as

$$\theta = \arctan\sqrt{\tan^2\gamma_x + \tan^2\gamma_y}. \qquad (8)$$

Figure 1b shows the instantaneous dip generated from a vertical slice of amplitude in Figure 1a, while Figure 7 presents a horizontal slice of the instantaneous azimuth from the same amplitude volume at 2.192 second. The orientation vector can also be used to derive other seismic attributes, such as curvature, or can guide a context window to calculate seismic attributes, such as dip-guided coherence.

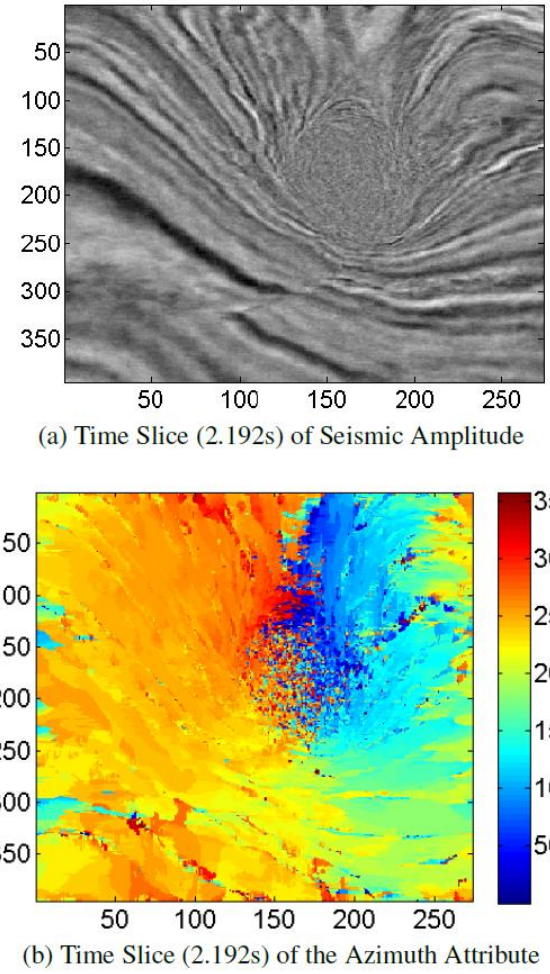

Figure 7: **Time Slice of Instantaneous Azimuth Attribute.** The time slice of amplitude (a) and its azimuth attribute (b).

Conclusion

This paper introduced a novel method of orientation analysis in a seismic image. One unique feature of our method is that it does not require a spatial context window. It is inspired by the neuronal mechanisms of the primary visual cortex for orientation perception. An array of log-Gabor filters is employed to simulate the neuronal responses of the orientation column, and an orientation vector field is generated to represent the orientation patterns in the seismic image. As demonstrated by the experiment, our proposed method is an effective way to perform the orientation pattern analysis, and has a number of potential applications for seismic interpretation.

Acknowledgments

Part of this paper has been previously presented at SEG 2013 annual meeting (Yu et. al, 2013). The authors would like to thank FairfieldNodal for permission to use the seismic data. This work is protected by US patent 8,265,876.

References

Aqrawi, A. A., and T. H. Boe, 2011, Improved fault segmentation using a dip guided and modified 3D Sobel filter: 81st Annual International Meeting, SEG, Expanded Abstracts, 999–1003.

Bakker, P., 2002, Image structure analysis for seismic Interpretation: Ph.D. thesis, Delft University of Technology.

Bakker, P., L. J. van Vliet, and P. W. Verbeek, 1999, Edge-preserving orientation adaptive filtering: Proceedings of the IEEE-CS Conference on Computer Vision and Pattern Recognition, IEEE, 535–540.

Barnes, A. E., 1996, Theory of 2D complex seismic trace analysis : Geophysics, **61**, 264–272.

Barnes, A. E., 2003, Shaded relief seismic attribute: Geophysics, **68**, 1281–1285.

Bovik, A., M. Clark, and W. Geisler, 1990, Multichannel texture anslysis using localized spatial filters: IEEE Transactions on Pattern Analysis and Machine Intelligence, **12**, 55–73.

Chopra, S., and K. J. Marfurt, 2007, Seismic attributes for prospect identif ication and reservoir characterization: SEG Geophysical Developments No. 11.

Daugman, J. G., 1980, Two-dimensional spectral analysis of cortical receptive field profiles: Vision Research, **20**, 847–856.

Field, D. J., 1987, Relations between the statistics of natural images and the response properties of cortical cells : Journal of the Optical Society of America, **4**, 2379–2394.

Fischer, S., F. Sroubek, L. Perrinet, R. Redondo, and G. Cristobal, 2007, Self-invertible 2D log-Gabor wavelets: International Journal of Computer Vision, **75**, 231–246.

Hubel, D. H., and T. N. Wiesel, 1959, Receptive fields of single neurones in the cat's striate cortex: The Journal of Physiology, **150**, 91–104.

Jain, A., N. Ratha, and S. Lakshmanan, 1997, Object detection using Gabor filters: Pattern Recognition, **30**, 295–309.

Lee, T. S, 1996, Image representation using 2D Gabor wavelets: IEEE Transactions on Pattern Analysis and Machine Intelligence, **18**, 959–971.

Luo, Y., W. G. Higgs, and W. S. Kowalik, 1996, Edge detection and stratigraphic analysis using 3-D seismic data: 66th Annual International Meeting, SEG, Expanded Abstracts, 324–327.

Marfurt, K. J., R. L. Kirlin, S. H. Farmer, and M. S. Bahorich, 1998, 3-D seismic attributes using a semblance-based algorithm: Geophysics, 63, 1150–1165.

Martinez, L. M., J. M. Alonso, R. C. Reid, and J. A. Hirsch, 2002, Laminar processing of stimulus orientation in cat visual cortex: The Journal of Physiology, 540, 321–333

Yu, Y., and Y. Choe, 2008, Neural model of disinhibitory interactions in the modified Poggendorff illusion: Biological Cybernetics, 98, 75–85.

Yu, Y., C. Kelley, and I. Mardanova, 2011, Automatic horizon picking in 3D seismic data using optical filters and minimum spanning tree: 81st Annual International Meeting, SEG, Expanded Abstracts, 965–958.

Yu, Y., C. Kelley, and I. Mardanova, 2013, Volumetric Seismic Dip and Azimuth Estimation with 2D Log-Gabor Filter Array: 83rd Annual International Meeting, SEG, Expanded Abstracts, 1357–1362.